Reconstruction of the Buried Homogenous Dielectric Cylinder by FDTD and Asynchronous Particle Swarm Optimization

Chung-Hsin Huang[1], Chien-Hung Chen[1], Chien-Ching Chiu[2] and Ching-Lieh Li[2]

[1] Department of Computer and Communication Engineering, Taipei College of Maritime Technology
Danshui Town, Taipei County, Taiwan, R.O.C.
chhuang@mail.tcmt.edu.tw, f1092@mail.tcmt.edu.tw

[2] Electrical Engineering Department, Tamkang University
Tamsui, Taiwan, R.O.C.
chiu@ee.tku.edu.tw, li@ee.tku.edu.tw

Abstract - In this paper, a time domain microwave imaging technique for reconstructing the electromagnetic properties of a buried homogeneous dielectric cylinder based on the finite difference time domain (FDTD) method and the asynchronous particle swarm optimization (APSO) are presented. The homogeneous dielectric cylinder with unknown electromagnetic properties is illuminated by transverse magnetic pulse and the scattered field is recorded outside. The idea is to minimize the errors between two E field data such that the location, shape and permittivity of the dielectric cylinder can be reconstructed through the APSO scheme. The first E field data are obtained in the forward problem by the FDTD code with fine grids to mimic the experiment measurement data, while the second E field data are obtained in the inverse problem by the FDTD code with coarse grids. The inverse problem is resolved by an optimization approach, and the global searching scheme APSO is then employed to search the parameter space. A set of representative numerical results is presented for demonstrating that the proposed approach is able to efficiently reconstruct the electromagnetic properties of homogeneous dielectric scatterer even when the initial guess is far away from the exact one. In addition, the effects of Gaussian noises on imaging reconstruction are also investigated.

Index Terms - APSO, FDTD, inverse scattering, subgridding FDTD, time domain.

I. INTRODUCTION

The objective of the inverse problem of the buried scatterer is to determine the electromagnetic properties of the scatterer from the scattering field outside. Due to the large domain of applications, such as non-destructive problems, medical imaging, geophysical prospecting and determination of underground tunnels and pipelines, etc, the inverse scattering problems related to the buried bodies have particular importance in the scattering theory. This kind of problem is expected to be more difficult due to the fact that the information about the buried unknown scatterer obtained by the limited–view measurement is less than the full-view measurement. Although the incompleteness of the measurement data and the multiple scattering of the scatterer bring out the intrinsic non-unique and ill-posedness of these problems that appear consequentially in the inverse scattering problems [1], the study can be applied in widespread use.

Most of the previously proposed inversion techniques for the inverse problems are formulated in the frequency domain [2-5]. However, the time domain scattering scheme is a potential alternative for the inverse problem because the data contain more information than those in the frequency case. Therefore, various time domain inversion approaches are proposed intensively in recent decades that could be briefly classified as the iterative approach: Born iterative method (BIM) [6], the distorted Born iterative method (DBIM) [7] and optimization approach [8, 9]. The inverse scattering problems are usually treated by the

traditional deterministic methods which are founded on a functional minimization via some gradient-type scheme. The major drawback of these kinds of deterministic methods is that the final reconstructed image is highly dependent on the initial trial guess [2, 3]. In general, they tend to get trapped in local minima when the initial trial solution is far from the exact one. Thus, some population-based stochastic methods, such as the genetic algorithm (GA) [4, 5, 10, 11], differential evolution (DE) [12-14], and particle swarm optimization (PSO) [14-17], are proposed to search the global extreme of the inverse problems to overcome the drawback of the deterministic methods. Rekanos et al. shows that asynchronous mode PSO (APSO) outperforms traditional synchronous mode PSO in reconstructed image quality. To the best of our knowledge, there is still no investigation using the APSO to reconstruct the electromagnetic imaging of homogeneous dielectric cylinders with arbitrary shape in half space based on a time domain method.

In this paper, the computational method combining the FDTD method [18] and the PSO algorithm with asynchronous updating scheme is presented. The forward problem is solved by the FDTD method, for which the subgridding technique [19] is implemented to closely describe the fine structure of the cylinder. The cross section shape of scatterer is parameterized by closed cubic spline expansion. The inverse problem is formulated into an optimization one and then the global searching scheme APSO is used to search the parameter space. In Section II, the theoretical formulation for the electromagnetic imaging is presented. The detail principle of the APSO and the way we applied them to the imaging problem are described. In Section III, numerical results for various dielectric objects are given, and the effect of noise is also investigated. Finally, some conclusions are drawn in Section IV.

II. THEORETICAL FORMULATION

Consider a 2-D homogeneous dielectric cylinder buried in a half space material medium as shown in Fig. 1. The cylinder is parallel to the z axis and is buried below a planar interface separating two homogeneous half spaces: the air (ε_1, μ_1) and the earth (ε_2, μ_2). The permittivity and permeability of the buried dielectric object are denoted

by (ε_3, μ_3), respectively. The dielectric object is illuminated by a line source with Gaussian pulse shape placed at two different positions sequentially denoted by Tx in the first layer, and then scattered waves are recorded at those points denoted simultaneously by Rx in the same layer.
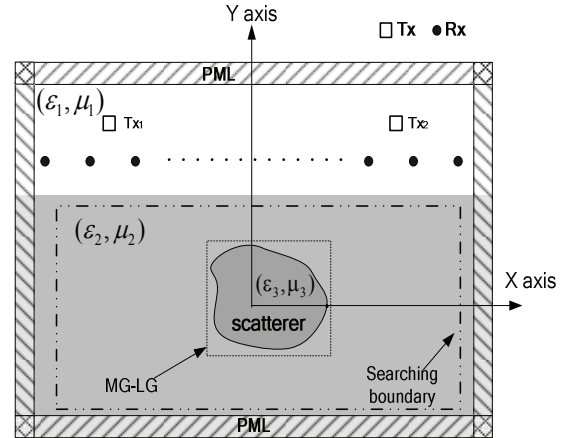

Fig. 1. Geometry for the inverse scattering of a dielectric cylinder of arbitrary shape in half space.

The shape of the cross section of the object is starlike and can be represented in polar coordinates with respect to the logic origin (X_O, Y_O) in the x-y plane as shown in Fig. 2. The computational domain is discretized by Yee cells. It should be mentioned that the computational domain is surrounded by the optimized perfect matching layers (PML) absorber [20] to reduce the reflection from the environment PML interface.
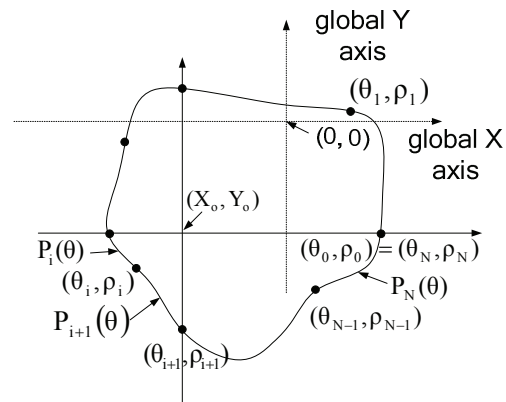

Fig. 2. A cylinder of arbitrary shape is described in terms of a closed cubic spline.

A. Forward problem

As mentioned in the abstract, the first E field data need to be obtained in the forward scattering problem by the FDTD code with fine grids to mimic the experimental measurement data. For the forward scattering problem the shape, location and permittivity of the dielectric cylinder to be determined is given first, and then the FDTD code is employed to calculate the scattered electric fields that are utilized to mimic the experiments. It should be noted that in the forward problem, the shape function $F(\theta)$ of the 2-D homogeneous dielectric cylinder buried in a half space is described by the trigonometric series as follows:

$$F(\theta) = \sum_{n=0}^{N/2} B_n \cos(n\theta) + \sum_{n=1}^{N/2} C_n \sin(n\theta). \qquad (1)$$

In order to closely describe the shape of the cylinder for both the forward and inverse scattering procedure, the subgridding technique is implemented in the FDTD code, the details are presented in later section.

B. Inverse problem

As mentioned in the abstract, the second E field data are obtained in the inverse problem by the FDTD code with coarse grids. As compared with the first E field data obtained in the forward scattering procedure, the inverse scattering problem can be formulated into an optimization problem. The proposed global searching APSO scheme is employed to reconstruct the location, shape and permittivity of the dielectric cylinder under test by minimizing the errors between two E filed data.

During the course of optimization process, the following objective function (OF) is defined for each candidate cylinder in the APSO scheme:

$$OF = \frac{\sum_{n=1}^{N_i} \sum_{m=1}^{M} \sum_{q=0}^{Q} \left| E_z^{exp}(n, m, q\Delta t) - E_z^{cal}(n, m, q\Delta t) \right|}{\sum_{n=1}^{N_i} \sum_{m=1}^{M} \sum_{q=0}^{Q} \left| E_z^{exp}(n, m, q\Delta t) \right|},$$

$$(2)$$

where E_z^{exp} is the electric field data to mimic the measurement as mentioned previously, and E_z^{cal} is the calculated electric fields in the inversion procedure, respectively. The N_i and M are the total number of the transmitters and receivers, respectively. Q is the total time step number of the recorded electric fields. The details of the proposed PSO are represented as follows.

C. Cubic spline interpolation technique

It should be noted that in the inverse problem, the shape function of the 2-D homogeneous dielectric cylinder is described by a cubic spline in this study instead of the trigonometric series described in the section of the forward problem. The cubic spline is more efficient in terms of the unknown number required to describe a cylinder of arbitrary cross section. By using the cubic spline the coordinates of local origin inside the cylinder serve as the searching parameter and can move around the searching space, which is impossible if the trigonometric series expansion is used in the inversion procedure.

As shown in Fig. 2, the cubic spline consists of the polynomials of degree 3 $P_i(\theta)$, $i = 1,2,\cdots,N$, which satisfy the following smooth conditions:

$$P_i(\theta_i) = P_{i+1}(\theta_i) \equiv \rho_i$$
$$P_i'(\theta_i) = P_{i+1}'(\theta_i), \quad i = 1,2,\cdots,N \qquad (3)$$
$$P_i''(\theta_i) = P_{i+1}''(\theta_i),$$

and

$$P_1(\theta_0) = P_N(\theta_N)$$
$$P_1'(\theta_0) = P_N'(\theta_N) \equiv \rho_N' \qquad (4)$$
$$P_1''(\theta_0) = P_N''(\theta_N).$$

Through the interpolation of the cubic spline, an arbitrary smooth cylinder can be easily described through the radius parameters $\rho_1, \rho_2, \cdots, \rho_N$ and the slope ρ_N', of which the details are referred to [21]. By combining the modified APSO and the cubic spline interpolation technique, we are able to reconstruct the microwave image efficiently.

It should be noted that the coordinates of local origin inside the cylinder plus the radiuses of the geometrical spline used to describe the shape of the cylinder will be determined by the asynchronous PSO scheme later.

D. **The modified synchronous particle swarm optimization (APSO)**

Particle swarm global optimization is a class of derivative-free, population-based and self-adaptive search optimization technique which we introduced by Kennedy and Eberhart [22]. Particles (potential solutions) are distributed throughout the searching space and their positions and velocities are modified based on social behavior. The social behavior in PSO is a population of particles moving towards the most promising region of the search space. Clerc [23] proposed the constriction factor to adjust the velocity of the particle for obtaining the better convergence; the algorithm was named as constriction factor method. PSO starts with an initial population of potential solutions that is randomly generated and composed N_p individuals (also called particles) which represents the dielectric constant, location and the geometrical radiuses of the cylinders.

After the initialization step, each particle of population has assigned a randomized velocity and position. Thus, each particle has a position and velocity vector, and moves through the problem space. In each generation, the particle changes its velocity by its best experience, called x_{pbest}, and that of the best particle in the swarm, called x_{gbest}.

Assume there are N_p particles in the swarm that is in a search space in D dimensions, the position and velocity could be determined according to the following equations (constriction factor method):

$$v_{id}^{k} = \chi \cdot \left(v_{id}^{k-1} + c_1 \cdot \varphi_1 \cdot \left(x_{pbest,id} - x_{id}^{k-1} \right) + c_2 \cdot \varphi_2 \cdot \left(x_{gbest,id} - x_{id}^{k-1} \right) \right)$$ (5)

$$x_{id}^{k} = x_{id}^{k-1} + v_{id}^{k} ,$$ (6)

where $\chi = \dfrac{2}{\left| 2 - \phi - \sqrt{\phi^2 - 4\phi} \right|}$, $\phi = c_1 + c_2 \geq 4$.

c_1 and c_2 are learning coefficients, used to control the impact of the local and global component in velocity equation (3). v_{id}^{k} and x_{id}^{k} are the velocity and position of the i-th particle in

the d-th dimension at k-th generation, φ_1 and φ_2 are both the random numbers between 0 and 1. It should be mentioned that the V_{max} method is also applied to control the particle's searching velocity and to confine the particle within the search space [24]. The value of V_{max} is set to be half of X_{max}, where X_{max} is the upper limits of the search space. Note that the V_{max} and X_{max} are maximum velocity and maximum distance, respectively. As an extreme case, if the maximum velocity V_{max} is set to X_{max}, the exploration to the inverse scattering problem space is not limited. Occasionally, the particles may move out of their search space. This problem could be remedied by applying the boundary condition to draw the foul particles back to the normal space. In this paper, we apply the "damping boundary condition" proposed by Huang and Mohan [25] to ensure the particles move within the legal search space. The key distinction between asynchronous PSO and a typical synchronous PSO is on the population updating mechanism. In the synchronous PSO, the algorithm updates all the particles velocities and positions using equations (5) and (6) at end of the generation. And then update the best positions, x_{pbest} and x_{gbest}. Alternatively, the updating mechanism of asynchronous PSO is that the new best position is found after each particle position updates, if the best position is better than the current best position. The new best position will be used in following particles swarm immediately. The swarm reacts more quickly to speedup the convergence because the updating occurs immediately after objective function evaluation for each particle.

The flowchart of the modified asynchronous PSO (APSO) is shown in Fig. 3. Asynchronous PSO goes through seven procedures as follows:

I. Initialize a starting population: Randomly generate a swarm of particles.

II. Calculate E fields by a home-made FDTD code.

III. Evaluate the population using objective function: The asynchronous PSO algorithm evaluates the objective function (2) for each individual in the population.
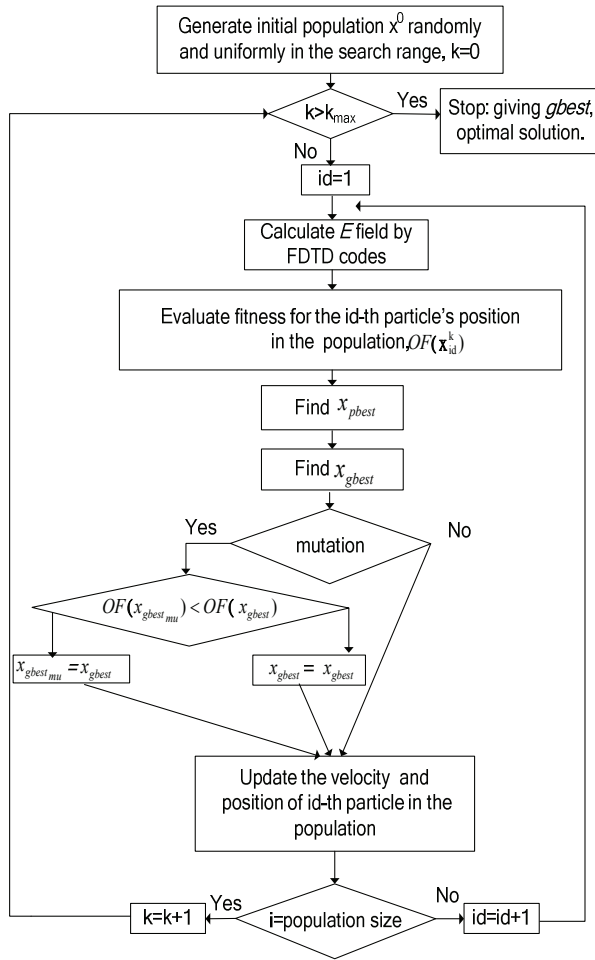
IV. Find x_{pbest} and x_{gbest}.

Fig. 3. The flowchart for the modified APSO.

V.   Mutation scheme: The particle swarm optimization (PSO) algorithm has been shown to converge rapidly during the initial stages of a global search, but when around global optimum, the search can become very slow. For this reason, mutation scheme is introduced in this algorithm to speed up the convergence when particles are around global optimum. The mutation scheme can also avoid premature convergences in the searching procedure and help the x_{gbest} escape from the local optimal position. As shown in Fig. 3, there is an additional competition between the x_{gbest} and $x_{pbest_{mu}}$. The current x_{gbest} will be replaced by the $x_{gbest_{mu}}$ if the $x_{gbest_{mu}}$ is

better than the current x_{gbest}. The $x_{gbest_{mu}}$ is generated by following way:

$$X_{gbest_{mu}} = \begin{cases} X_{gbest} - \varphi_3 \cdot \left[c_3 - (c_3 - c_4) \cdot \dfrac{k}{k_{max}} \right] \cdot (x_{max} - x_{min}), \text{ if } \varphi_{mu} < 0.5 \\ X_{gbest} + \varphi_3 \cdot \left[c_3 - (c_3 - c_4) \cdot \dfrac{k}{k_{max}} \right] \cdot (x_{max} - x_{min}), \text{ if } \varphi_{mu} \geq 0.5 \end{cases}, (7)$$

where c_3 and c_4 are the scaling parameter. φ_3 and φ_{mu} are both the random numbers between 0 and 1. k is the current iteration number. k_{max} is the maximum iteration number. x_{max} and x_{min} are the upper limit and lower limit of the search space, respectively.

VI.   Update the velocity and position.
VII.   Stop the process and print the best individual if the termination criterion is satisfied, else go to step II.

III. NUMERICAL RESULTS

In this section, we report some numerical results using the method described in Section II. As shown in Fig. 1, the problem space is divided in 128×68 grids with the grid size $\Delta x = \Delta y = 5.95$ mm. The homogeneous dielectric cylinder is buried in lossless half space ($\sigma_1 = \sigma_2 = 0$). The transmitters and receivers are placed in free space above the homogeneous dielectric. The permittivities in region 1 and region 2 are characterized by $\varepsilon_1 = \varepsilon_0$ and $\varepsilon_2 = 2.3\varepsilon_0$, respectively, while the permeability μ_0 is used for each region, i.e., only non-magnetic media are concerned here. The distance between the half space interface and the original cylinder is 89.2mm. The cylindrical object is illuminated by a transmitter at two different positions, N_i=2, which are located at the (-143mm, 178.5mm) and (143mm, 178.5mm), respectively. The scattered E fields for each illumination are collected at the fifteen receivers, M = 15, which are equally separated by 47.8 mm along the distance of 48 mm from the half space interface. The excitation waveform $I_z(t)$ of the transmitter is the Gaussian pulse, given by:

$$I_z(t) = \begin{cases} Ae^{-\alpha(t-\beta\Delta t)^2} & , t \le T_w \\ 0 & , t > T_w \end{cases},$$ (8)

where $\beta = 32$, $A = 1000$, $\Delta t = 13.337\,ps$,

$T_w = 2\beta\Delta t$, and $\alpha = \left(\dfrac{1}{4\beta\Delta t}\right)^2$.

The time duration is set to $300\,\Delta t$ ($s = 300$). Note that in order to describe the shape of the cylinder more accurately, the subgridding FDTD technique is employed both in the forward scattering (1:9) and the inverse scattering (1:5) parts – but with different scaling ratios as indicated in the parentheses. For the forward scattering, the E fields generated by the FDTD with finer subgrids are used to mimic the experimental data in (2).

The reconstruction ideas are carried out through a home-made Fortran program that runs on an Intel PC (2.83 GHz/ 2G memory /500 G).

Three examples are investigated for the inverse scattering of the proposed structure by using the modified APSO. There are twelve unknown parameters to retrieve, which include the coordinates of local origin (X_O, Y_O) inside the cylinder, the radius ρ_i, $i = 1, 2, \cdots, 8$ of the shape function and the slope ρ'_N plus the relative permittivity of the object, $\varepsilon_r = \varepsilon_3 / \varepsilon_0$. Very wide searching ranges are used for the modified APSO to optimize the cost function given by (2). The parameters and the corresponding searching ranges are listed as follows: $-208.3\text{mm} \le X_O \le 208.3\text{mm}$, $-137.8\text{mm} \le Y_O \le 77.4\text{mm}$, $0\text{mm} \le \rho_i \le 71.4\text{mm}$, $i = 1, 2, \cdots, 8$, $-1 \le \rho'_N \le 1$ and $1 \le \varepsilon_r \le 16$. The relative coefficients of the modified APSO are set as below: The learning coefficients, c_1 and c_2, are set to 2.8 and 1.3, respectively. The mutation probability is 0.4 and the population size is set to 30.

The first example, a simple circular cylinder is tested, of which the shape function $F(\theta)$ is chosen to be $F(\theta) = 35.7$ mm, and the relative permittivity of the object is $\varepsilon_r = 3.7$. The convergence curves of objective function versus the generation as the proposed APSO being executed seven times out of ten by using different

tables of random numbers are shown in Fig. 4. The small converged values show the robustness for the APSO scheme applied this topic.
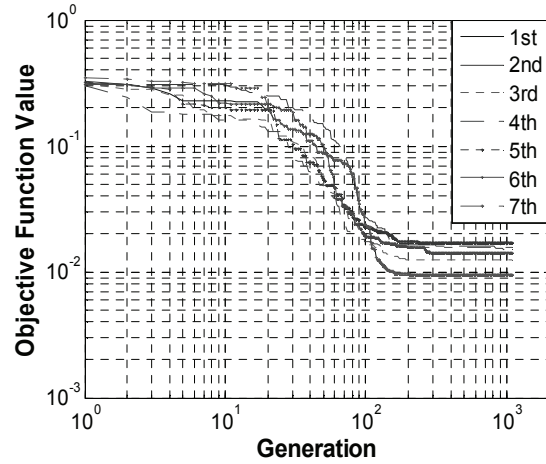

Fig. 4. The objective function value versus generations for example 1 using the Gaussian pulse illumination as the APSO is executed seven times.
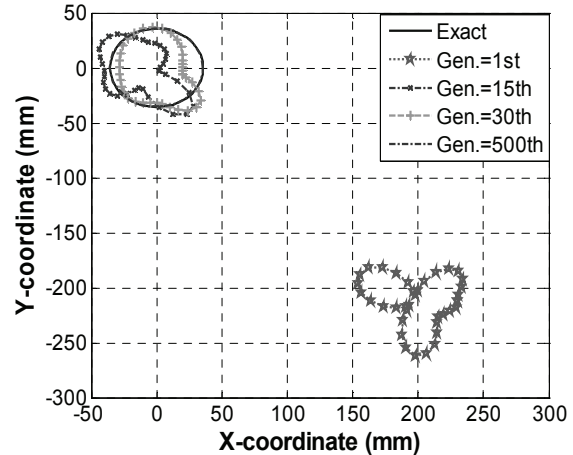

Fig. 5. The reconstructed shape of the cylinder at different generations for example 1.

The reconstructed shape function of the best population member (particle) is plotted in Fig. 5 for different generation. The discrepancy of shape Function (DF) of the reconstructed shape $F^{cal}(\theta)$ and the discrepancy of dielectric constant (DIPE) of ε_r^{cal} with respect to the exact values versus the generation are shown in Figure 6. Here, DF and DIPE are defined as

$$DF = \{\frac{1}{N'}\sum_{i=1}^{N'}[F^{cal}(\theta_i) - F(\theta_i)]^2 / F^2(\theta_i)\}^{1/2} ,$$

(9)

$$DIPE = \frac{|\varepsilon_r^{cal} - \varepsilon_r|}{\varepsilon_r} ,$$

(10)

where the N' is set to 360. The r.m.s. error DF is about 0.84% and DIPE= 0.21%. It is seen that the reconstruction is good.
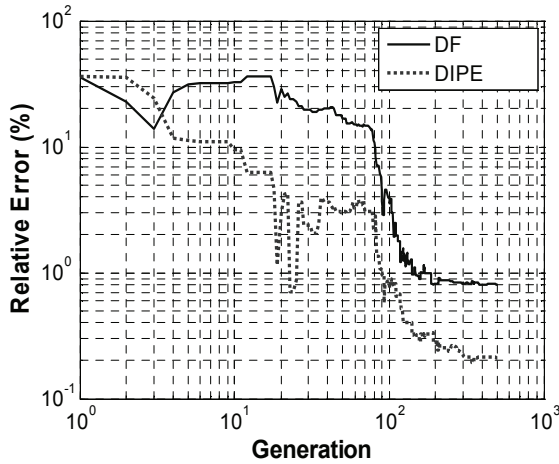

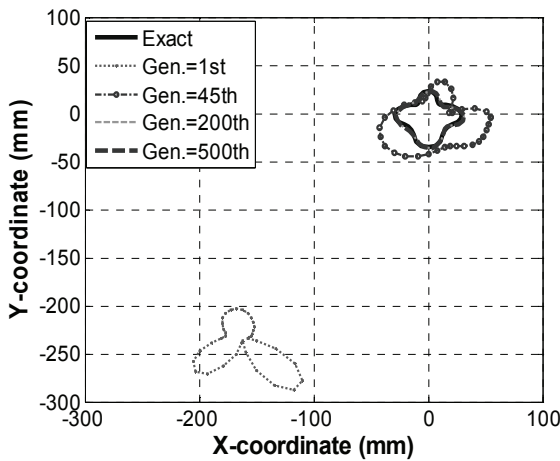Fig. 6. Shape error and permittivity error versus generation for example 1.

Fig. 7. The reconstructed cross section of the cylinder of example 2 at different generations.

The reconstructed images for different generations and the relative error of the second example are shown in Figs. 7 and 8, respectively. The shape function of this object is given by $F(\theta) = 23.8 - 5.95\sin(\theta) + 5.95\cos(4\theta)$ mm and the

relative permittivity of the object is $\varepsilon_r = 6.2$. Figure 8 shows that the relative errors of the shape and the permittivity decrease quickly and good convergences are achieved within 200 generations. It also shows that the permittivity converges faster than the shape function does. The r.m.s. error DF is about 6.65% and DIPE=2.21% in the final generation. From the reconstructed results of this example, we conclude the proposed method is able to reconstruct buried dielectric cylinder successfully when the dielectric object is with high-contrast permittivity.
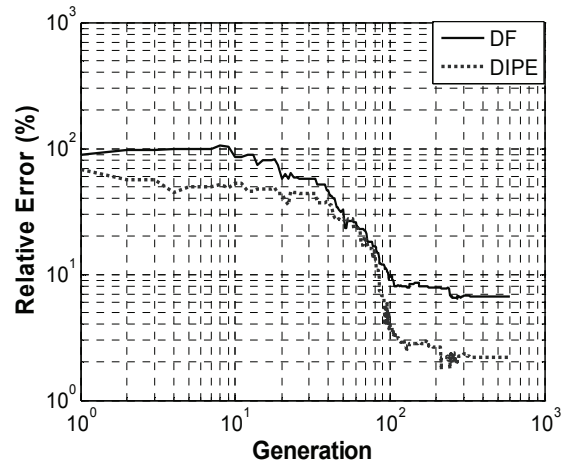

Fig. 8. Shape-function error and permittivity error versus generations for example 2.

In the final example, let us consider the problem for dielectric cylinders with high permittivity. The shape function of this object is given by $F(\theta) = 29.7 + 5.95\sin(2\theta) + 5.95\cos(3\theta) - 5.95\sin(3\theta)$ mm and the relative permittivity of the object is $\varepsilon_r = 3$. The reconstructed images at different generations and the relative error of the final example are shown in Fig. 9 and Fig 10, respectively. As shown in Figure 10, the r.m.s. error DF is about 5% and DIPE=0.20% in the final generations. In order to investigate the sensitivity of the imaging algorithm against random noise, the additive white Gaussian noise of zero mean with standard deviation σ_g is added into the scattered electric fields to mimic the measurement errors. The relative noise level (RNL) is defined as:

$$RNL = \frac{\sigma_g}{\sqrt{\dfrac{\sum\limits_{n=1}^{Ni}\sum\limits_{m=1}^{M}\sum\limits_{k=0}^{K}\left|E_z^{exp}(n,m,k\Delta t)\right|^2}{(N_i)(M_i)(K-1)}}} \quad .$$

(11)

The relative noise levels of 10^{-4}, 10^{-3}, 10^{-2}, 10^{-1}, 0.2 and 0.5 are used. Fig. 11 shows the reconstructed results under the condition that the scattered E fields to mimic the measurement data are contaminated by the noise. It could be observed that good reconstruction has been obtained for both the relative permittivity and shape of the dielectric cylinder when the relative noise level is below 10^{-1}.

Fig. 11. Shape error and relative permittivity errors as functions of RNL.

IV. CONCLUSION

In this paper, a new numerical approach to microwave imaging of homogeneous dielectric scatterer with arbitrary cross section in time domain has been presented. Scattering fields are obtained by FDTD method. The subgridding scheme is employed to closely describe the shape of the cylinder for the FDTD method. The approach has been formulated as a global nonlinear optimization problem and a modified asynchronous PSO has been applied. It has been shown that the properties of the dielectric object can be successfully reconstructed even when the dielectric object with fairly large permittivity and the Born approximation is no longer valid. In our study, good reconstructed results are obtained even when the initial guess is far from the exact one, while the gradient-based methods often get stuck in a local extreme. Numerical results have been carried out and good reconstruction has been obtained even in the presence of white Gaussian noise in experimental data.
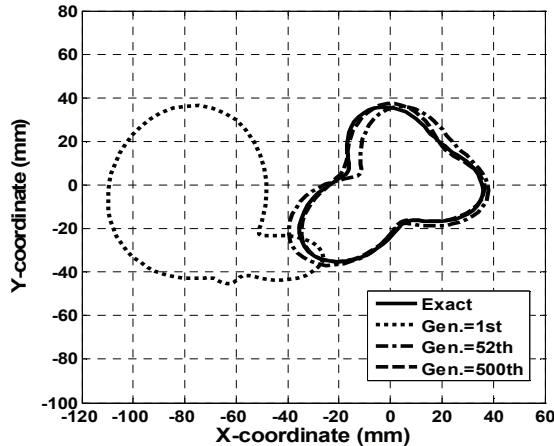

Fig. 9. The reconstructed cross section of the cylinder of example 3 at different generations.

Fig. 10. Shape-function error and permittivity error versus generations for example 3.
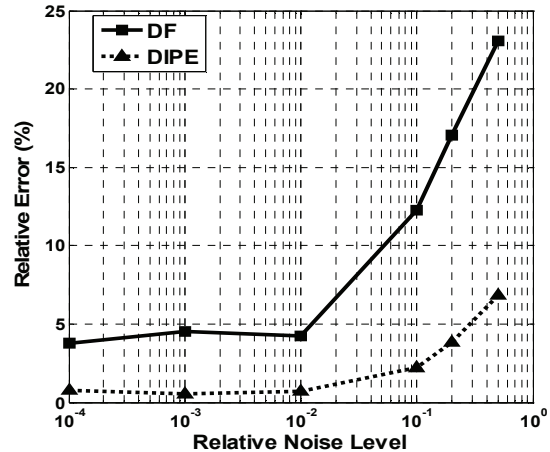
REFERENCES

[1] D. Colton and R. Kress, *Inverse Acoustic and Electromagnetic Scattering Theory*, Springer-Verlag, New York, 1992.

[2] F. Yaman, S. Simçsek, "Neural network approach to determine nonsmooth one-dimensional profiles in inverse scattering theory," *Microwave and Optical Technology Letters,* vol. 49, no. 12, pp. 3158-3162, Dec. 2007.

[3] C. H. Sun, C. L. Liu, K. C. Chen, C. C. Chiu, C. L. Li, and C. C. Tasi, "Electromagnetic transverse electric wave inverse scattering of a partially immersed conductor by steady-state genetic algorithm," *Electromagnetics.* vol. 28, no. 6, pp. 389-400, Aug. 2008.

[4] M. Donelli, G. Franceschini, A. Martini, and A. Massa, "An integrated multiscaling strategy based on a particle swarm algorithm for inverse scattering problems," *IEEE Transactions on Geoscience and Remote Sensing,* vol. 44, no. 2, pp. 298-312, Feb. 2006.

[5] W. Chien, C. H. Sun, and C. C. Chiu, "Image reconstruction for a partially immersed imperfectly conducting cylinder by genetic algorithm," *International Journal of Imaging Systems and Technology,* vol. 19, pp. 299-305, Dec. 2009

[6] M. Moghaddam and W. C. Chew, "Study of some practical issues in inversion with the Born iterative method using time-domain data," *IEEE Transactions on Antennas and Propagation*, vol. 41, no. 2, pp. 177-184, Feb. 1993.

[7] W. H. Weedon, *Broadband microwave inverse scattering: Theory and experiment*, Ph.D. dissertation, University of Illinois at Urbana-Champaign, 1994.

[8] I. T. Rekanos, "Time-domain inverse scattering using Lagrange multipliers: an iterative FDTD-based optimization technique," *Journal of Electromagnetic Waves and Applications*, vol. 17, no. 2, pp. 271-289, 2003.

[9] T. Takenaka, H. Jia, and T. Tanaka, "Microwave imaging of electrical property distributions by a forward-backward time-stepping method," *Journal of Electromagnetic Waves Application*, vol. 14, pp. 1609–1625, 2000.

[10] X. M. Zhong, C Liao, and W. Chen, "Image reconstruction of arbitrary cross section conducting cylinder using UWB pulse," *Journal of Electromagnetic Waves Application,,* vol. 21, no. 1, pp. 25-34, 2007.

[11] C. H. Huang, C. C. Chiu, C. L. Li, and Y. H. Li, "Image reconstruction of the buried metallic cylinder using FDTD method and SSGA," *Progress In Electromagnetics Research*, vol. 85, pp. 195-210, 2008.

[12] K. A. Michalski, "Electromagnetic imaging of circular-cylindrical conductors and tunnels using a differential evolution algorithm," *Microwave and Optical Technology Letters*, vol. 27, no. 5, pp. 330–334, Dec. 2000

[13] A. Semnani, M. Kamyab, and I. T. Rekanos, "Reconstruction of one-dimensional dielectric scatterers using differential evolution and particle swarm optimization," *IEEE Geoscience and Remote Sensing Letters*, vol. 6, no. 4, pp. 671-675, Oct. 2009.

[14] I. T. Rekanos, "Shape reconstruction of a perfectly conducting scatterer using differential evolution and particle swarm optimization, " *IEEE Transactions on Geoscience and Remote Sensing*, vol. 46, no. 7, pp. 1967-1974, July 2008.

[15] M. Donelli and A. Massa, "Computational approach based on a particle swarm optimizer for microwave imaging of two-dimensional dielectric scatterers," *IEEE Transactions on Microwave Theory and Techniques*, vol. 53, no. 5, pp. 1761 - 1776, May. 2005.

[16] T. Huang and A. S. Mohan, "Application of particle swarm optimization for microwave imaging of lossy dielectric objects," *IEEE Antenna and Propagation Society International Symposium Digest*, pp. 852 – 855, 2005.

[17] C. H. Huang, C. C. Chiu, C. L. Li, and K. C. Chen, "Time domain inverse scattering of a two-dimensional homogenous dielectric object with arbitrary shape by particle swarm optimization," *Progress In Electromagnetic Research,* vol. 82, pp. 381-400, 2008.

[18] A. Taflove and S. Hagness, *Computational Electrodynamics: The Finite-Difference Time-Domain Method*, Artech House, Boston, MA, 2000.

[19] M. W. Chevalier, R. J. Luebbers, and V. P. Cable, "FDTD local grid with material traverse," *IEEE Trans. Antennas and Propagation,* vol. 45, no. 3, March 1997.

[20] C. L. Li, C.-W. Liu, and S. H. Chen, "Optimization of a PML absorber's conductivity profile using FDTD," *Microwave and Optical Technology Letters*, vol. 37, no. 5, pp. 69-73 , Jun. 2003

[21] C. de Boor, *A Practical Guide to Splines*, Springer-Verlag, New York, 1978.

[22] J. Kennedy and R. C. Eberhart, "Particle swarm optimization," *Proceedings of the IEEE International Conference on Neural Network*, pp. 1942-1948, 1995.

[23] M. Clerc, "The swarm and the queen: towards a deterministic and adaptive particle swarm optimization," *Proceedings of Congress on Evolutionary Computation*, Washington, DC, pp. 1951-1957, 1999.

[24] A. Carlisle and G. Dozier, "An Off-The-Shelf PSO," *Proceedings of the Workshop on Particle Swarm Optimization*, pp.1-6, 2001.

[25] T. Huang and A. S. Mohan, "A hybrid boundary condition for robust particle swarm. optimization," *IEEE Antennas and Wireless Propagation Letters*, vol. 4, pp.112-117, 2005.

Chung-Hsin Huang was born in Tucheng, Taiwan, Republic of China, on February 1, 1980. He received his M.S.E.E. and Ph.D. degrees in electrical engineering from Tamkang University, Taipei, Taiwan, in 2004 and 2009 respectively. He is currently an Assistant Professor with the Department of Computer and Communication Engineering, Taipei College of Maritime Technology. His current research interests include inverse scattering problem, optimization methods, dielectric material characterization, and wireless communications.

Chien-Hung Chen was born in Kaohsiung, Taiwan, Republic of China, on March 8, 1971. He received his M.S.E.E. and Ph.D. degrees in electrical engineering from Tamkang University, Taipei, Taiwan, in 1999 and 2006 respectively. He is currently an Assistant Professor with the Department of Computer and Communication Engineering, Taipei College of Maritime Technology. His current research interests include indoor wireless communications and numerical techniques in electromagnetics.

Chien-Ching Chiu was born in Taoyuan, Taiwan, Republic of China, on January 23, 1963. He received the B.S.C.E. degree from National Chiao Tung University, Hsinchu, Taiwan, in 1985 and his M.S.E.E. and Ph.D. degrees from National Taiwan University, Taipei, Taiwan, in 1987 and 1991 respectively. From 1987 to1989, he served in the ROC Army Force as a communication officer. In 1992, he joined the faculty of the Department of Electrical Engineering, Tamkang University, where he is now a Professor. He was a visiting scholar at the MIT and University of Illinois, Urbana from 1998 to 1999. His current research interests include microwave imaging, numerical techniques in electromagnetic, and indoor wireless communications.

Ching-Lieh Li was born November 24, 1963, in Pingtun, Taiwan. He received the B.S. degree from National Taiwan University, Taipei, Taiwan, in 1985, and the M.S. and Ph.D. degrees from Michigan State University, East Lansing, in 1990 and 1993, respectively, all in electrical engineering.

From 1989 to 1993, he was a Research Assistant in the Electrical Engineering Department, Michigan State University, where he worked on the measurement techniques for determining the electromagnetic properties of materials. In 1993, he joined the Electrical Engineering Faculty at Tamkang University, Taipei, Taiwan. Currently, his research activities involve inverse scattering problem, and microstrip antenna design and dielectric material characterization. His areas of special interest include theoretical and computational electromagnetics, and application of various optimization schemes such as SSGA, PSO, DDE, Taguchi method in electromagnetics.